Front. Earth Sci. 2013, 7(3): 257–270
DOI 10.1007/s11707-013-0368-9

REVIEW ARTICLE

The calibration methods for Multi-Filter Rotating Shadowband Radiometer: a review

Maosi CHEN (✉)[1], John DAVIS[1], Hongzhao TANG[1], Carolyn OWNBY[1], Wei GAO[1,2]

1 USDA UV-B Monitoring and Research Program, Natural Resource Ecology Laboratory, Colorado State University, Fort Collins, CO 80521, USA
2 Department of Ecosystem Science and Sustainability, Colorado State University, Fort Collins, CO 80521, USA

Abstract The continuous, over two-decade data record from the Multi-Filter Rotating Shadowband Radiometer (MFRSR) is ideal for climate research which requires timely and accurate information of important atmospheric components such as gases, aerosols, and clouds. Except for parameters derived from MFRSR measurement ratios, which are not impacted by calibration error, most applications require accurate calibration factor(s), angular correction, and spectral response function(s) from calibration. Although a laboratory lamp (or reference) calibration can provide all the information needed to convert the instrument readings to actual radiation, in situ calibration methods are implemented routinely (daily) to fill the gaps between lamp calibrations. In this paper, the basic structure and the data collection and pretreatment of the MFRSR are described. The laboratory lamp calibration and its limitations are summarized. The cloud screening algorithms for MFRSR data are presented. The in situ calibration methods, the standard Langley method and its variants, the ratio-Langley method, the general method, Alexandrov's comprehensive method, and Chen's multi-channel method, are outlined. The reason that all these methods do not fit for all situations is that they assume some properties, such as aerosol optical depth (AOD), total optical depth (TOD), precipitable water vapor (PWV), effective size of aerosol particles, or angstrom coefficient, are invariant over time. These properties are not universal and some of them rarely happen. In practice, daily calibration factors derived from these methods should be smoothed to restrain error.

Keywords Multi-Filter Rotating Shadowband Radiometer (MFRSR), calibration, review

Received March 5, 2013; accepted March 8, 2013

E-mail: chenms@uvb.nrel.colostate.edu

1 Introduction

Climate change has received more and more concern in the last few decades. The amount and distribution variation of gaseous and particle components in the Earth's atmosphere that alter the radiative forcing balance are believed to be the main cause of such change. In the Intergovernmental Panel on Climate Change (IPCC) report (AR4), water vapor is considered the most important greenhouse gas (positive radiative forcing), and carbon dioxide (CO_2) is the second-most important one. Trace gases such as methane, nitrous oxide, ozone, and several others also contribute to the greenhouse effect. Although water vapor has positive radiative forcing, Ramanathan et al. (1989) found that clouds had a net global cooling effect on the earth based on the radiative forcing data from the spaceborne Earth Radiation Budget Experiment (ERBE). The contribution of aerosols to overall radiative forcing is significant as well, although the effect is highly variable due to high uncertainty of the mean aerosol radiative forcing (Feister et al., 2007). Charlson et al. (1992) showed that aerosol particles can scatter short wavelength solar radiation and modify the shortwave reflective properties of clouds, which lead to increased planetary albedo and have cooling effects on the planet. The magnitude of the global average of the aerosol radiative forcing is comparable to that of anthropogenic greenhouse gas forcing but opposite in sign. However, the different geographical and temporal distribution of these forcings precludes any simple compensation. Ramanathan et al. (2001) concluded that increased albedo caused by aerosols leads to large reductions of solar irradiance reaching the Earth's surface, changing the atmospheric temperature profile and the pattern of rainfall.

In addition to the changing temperature profile effect of climate change, the change in shortwave solar irradiance reaching the Earth's surface because of variation in clouds, gases, and aerosols in the atmosphere is also significant.

Surface radiative energy budget studies must know the effect of clouds and other interference on shortwave irradiance (Long and Ackerman, 2000). Solar radiation in the visible region is the driving force for photosynthesis (Monteith and Unsworth, 2008), while that in the ultraviolet region (especially in the UV-B section) is considered an adverse condition for vegetation growth and crop yield accumulation (Kakani et al., 2003a, 2003b) and human and animal health (Caldwell et al., 1986; Teramura et al., 1990; Madronich, 1993). Both solar irradiance and aerosols have direct impact on human health (Lighty et al., 2000). Aerosols also impact surface visibility conditions, as radiation reflected from aerosol particulates contributes to direct irradiance (Chow et al., 1994).

In the annual report of the Atmospheric Radiation Measurement (ARM) Climate Research Facility (FY_2011)[1)], it is concluded that global climate models (GCMs) are one of the primary tools for simulating climate change. These models require knowledge of clouds and aerosols, and their effects on the Earth's energy balance. Remote sensing of solar radiation (ground-based, airborne, or satellite-based) is widely used for retrieving properties of these parameters. The validation of satellite retrieval algorithms for surface irradiance requires accurate surface measurement (Wielicki et al., 1995). Ground based sun photometric measurement can also be used to produce aerosol, ozone, UV radiation, precipitable water vapor, and cloud climatology (Leontieva and Stamnes, 1996; Kiedron et al., 1999; Michalsky et al., 2001a; Alexandrov et al., 2002b, 2009; di Sarra et al., 2008; Mazzola et al., 2010; Kassianov et al., 2011; Yin et al., 2011). There are various types of instruments that provide sun photometric measurements, for example: (i) CIMEL sun radiometers, which are the key instruments at Aerosol Robotic Network (AERONET) (Holben et al., 1998) sites; and (ii) Multi-Filter Rotating Shadowband Radiometers (MFRSR) (Alexandrov et al., 2008). An advantage of the MFRSR is that it can be operated automatically and its cost is relatively low, making the construction of networks for distributed data collection feasible. The growing international deployment of the MFRSR makes it a potentially important tool for climate research (Alexandrov et al., 2002).

Except for the direct/diffuse and total/diffuse MFRSR component ratios which cancel out the dependency on absolute calibration (Kaskaoutis et al., 2008), the successful application of MFRSR measurements relies on stable and accurate calibration, which converts the instrument reading to actual radiation, and gives the angular correction and spectral response function. The calibration parameters determined before deployment can shift dramatically and quickly in the field, which requires frequent recalibration (laboratory or in situ) to produce reliable radiation measurements.

In this paper, we present a description of the ultraviolet and visible versions of MFRSR instrument, its data collection, and issues related to the challenge of calibration. We review the published calibration efforts, including both laboratory lamp and in situ calibration methods.

2 The UV- and VIS-MFRSR

The VIS-MFRSR (Fig. 1) is the visible version of the MFRSR. It is environmentally sealed and thermally stabilized at around 40°C, and uses state-of-the-art interference filter photodiode detectors. It contains six narrowband channels (415, 500, 615, 673, 870, and 940 nm), each with a 10 nm full-width at half maximum (FWHM) bandwidth. The seventh channel is an unfiltered silicon (Si) photodiode responsive to 300–1040 nm. The Lambertian diffuser of the VIS-MFRSR is made of Spectralon®.

The UV-MFRSR is the ultraviolet version of the MFRSR. It is environmentally sealed and thermally stabilized at around 42°C, and uses seven state-of-the-art interference filter photodiode detectors (center wavelengths at 300, 305, 311, 317, 325, 332, and 368 nm), each with a 2 nm FWHM bandwidth (Bigelow et al., 1998). The 300 and 305 channels use silicon-carbide (SiC) photodiodes, and the 311 through 368 channels use silicon (Si) photodiodes. The Lambertian diffuser of the UV-MFRSR is made of Teflon®.

According to Alexandrov et al. (2008), the programs that are running MFRSR networks in the United States include the USDA UV-B Monitoring and Research Program (UVMRP) (Bigelow et al., 1998), the DOE Atmospheric Radiation Measurement (ARM) Program (Ackerman and Stokes, 2003), the NOAA Surface Radiation (SURFRAD) Network (Augustine et al., 2005), and the NASA Solar Irradiance Research Network (SIRN).

The basic geometry of the MFRSR can be seen in Fig. 1 and Fig. 2.

The shadow-band is an arched metal strip that blocks a strip of sky with an umbral angle (Zp) of 3.27°, which is more than sufficient to block the solar disk (Harrison et al., 1994b). A self-contained microprocessor calculates the solar position by using an approximation for the solar ephemeris, which controls the rotation of the shadow-band to certain positions. The stepping precision and error may limit accuracy to $\pm 0.3°$. After the instrument is installed at a site, a onetime adjustment for latitude and azimuth alignment to the Earth's pole is performed.

Unlike a sun photometer, the MFRSR does not measure the direct beam irradiance directly. Instead, the MFRSR

1) http://www.arm.gov/publications/annual-reports/docs/doe-sc-arm-11-024.pdf?id = 94

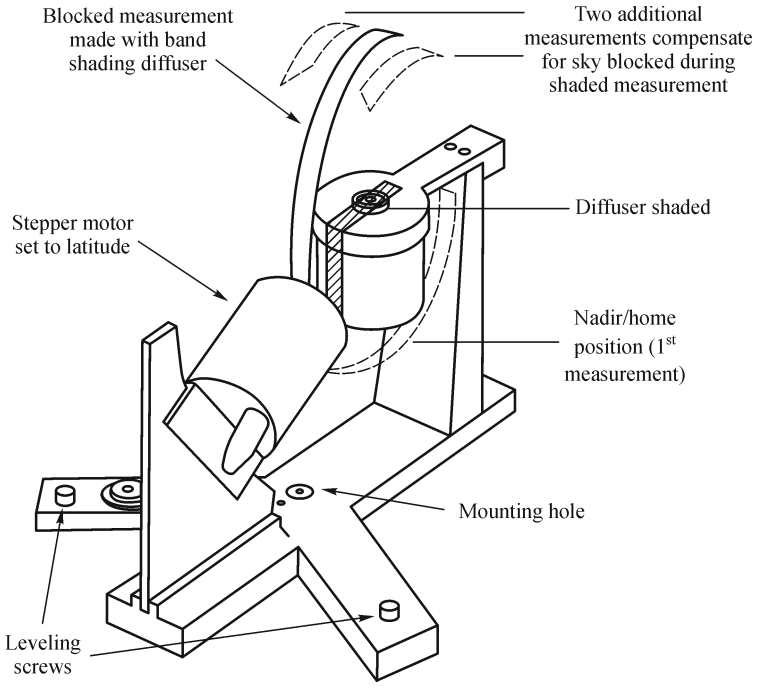

Fig. 1 Basic geometry of a MFRSR (Hodges and Michalsky, 2011)

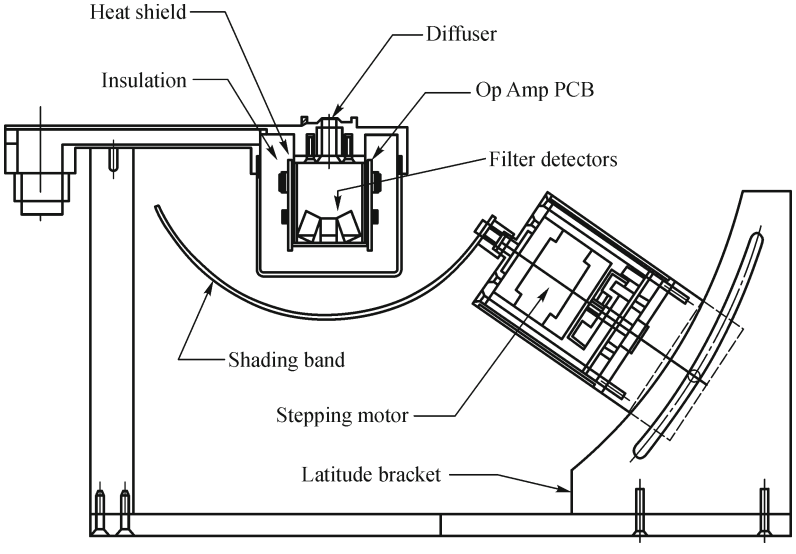

Fig. 2 Cut-out view of a MFRSR (Hodges and Michalsky, 2011)

derives the direct beam from its principal measurements. To collect one data record, a set of four measurements are taken (Hodges and Michalsky, 2011):

(i) The initial measurement (total horizontal, *t_hor*) is taken when the shadow-band is in the home position (Fig. 1 Nadir/home position);

(ii) The first of two side-band measurements (first side band, *fsb*) is taken when the shadow-band is 9° off the sun blocking direction (Fig. 1: Two additional measurements compensate for sky blocked during shaded measurement);

(iii) The sun-blocked measurement (*blk*) is taken (Fig. 1: Blocked measurement made with band shading diffuser);

(iv) The second of two side-band measurements (second side band, *ssb*) is taken when the shadow-band is 9° off the sun blocking direction (the other side of the step (2), Fig. 1: Two additional measurements compensate for sky blocked during shaded measurement).

These four measurements are made every 20 s (15 s for

UV-MFRSR) and averaged into 3-min intervals for the USDA UVMRP, and 2-min intervals for the SURFRAD network.

2.1 Dark current bias removal (offset correction)

Extraneous voltages that are not the result of radiation incidence but the inherent noise of the instrument should be removed (Bigelow et al., 1998; Hodges and Michalsky, 2011). Under normal operations, the nighttime data (voltages measured one hour prior to and one hour after the time of minimum solar elevation over a three-day period preceding the current data processing day) are averaged to estimate this offset, which is subtracted from all the measurements in the daytime before any further calculation.

The measurements of steps (2) and (4) permit a first-order correction for the excess sky blocked by the shadowband for the step (3) measurement. The diffuse horizontal (*dif_hor*) is expressed as

$$dif\_hor = blk + [t\_hor - (fsb + ssb)/2]. \quad (1)$$

The direct horizontal (*dir_hor*) is expressed as

$$dir\_hor = t\_hor - dif\_hor. \quad (2)$$

2.2 Cosine response correction

Radiation incident on a flat horizontal surface originating from a point source with a defined zenith position will have an intensity value proportional to the cosine of the zenith angle of incidence. When the sun is directly overhead, the theoretical cosine correction is one. This is called the cosine-response. Ideally, spectroradiometers are designed to have a directional response which is exactly the same as the cosine-response. However, the actual instruments rarely match this ideal (Seckmeyer and Bernhard, 1993; Michalsky et al., 1995; Feister et al., 1997). The magnitude of this discrepancy (known as cosine error) can vary from a few percent to 10% or 20%, depending on the atmospheric conditions (i.e. cloudiness and aerosol optical depth (Feister et al., 1997)) and the characteristics of the system (Blumthaler and Bais, 1996; Bais, 1997; Bais et al., 1998). The cosine correction table, which considers errors regarding both the azimuth angle and zenith angle of incidence, is provided for each MFRSR by the manufacturer or the calibration laboratory. With this table, one obtains the cosine corrected direct (*cor_dir_hor*) and diffuse (*cor_dif_hor*) horizontals:

$$\begin{aligned} cor\_dif\_hor &= dif\_hor/(diffuse\ \cos\ ine\ correction), \\ cor\_dir\_hor &= dir\_hor/(direct\ \cos\ ine\ correction). \end{aligned} \quad (3)$$

The cosine corrected total horizontal (*cor_t_hor*) is the sum of these two values:

$$cor\_t\_hor = cor\_dif\_hor + cor\_dir\_hor. \quad (4)$$

Now, the direct normal (*dir_norm*) is calculated as:

$$dir\_norm = cor\_dir\_hor/\cos\theta, \quad (5)$$

where, the θ is the zenith angle of incidence or solar zenith angle.

The measurements or derived quantities in Eqs. (1) to (5) are voltages. The conversion of voltage to irradiance requires a calibration factor (c):

$$I_\lambda = V_\lambda / c_\lambda, \quad (6)$$

where, λ represents the MFRSR channel or effective wavelength.

3 Laboratory lamp calibration

3.1 Major tasks of laboratory lamp calibration

There are many facilities that provide laboratory calibration, such as the Central UV Calibration Facility (CUCF), NOAA, Boulder, Colorado; Yankee Environmental Systems (YES), Inc.; and the Atmospheric Radiation Measurement Program (ARM) Southern Great Plains (SGP) Central Facility (CF). Generally, laboratory calibration includes three important tasks:

(i) Standard lamp calibration, which determines the calibration factor c_λ for each channel;

(ii) Angular response determination, which generates angular correction tables; and

(iii) Spectral Response Function (SRF) of each filter detector (channel) determination, which is also known as the filter function.

The second and third tasks can only be determined via lamp calibration, while the first part can also be determined via in situ calibration methods or via calibration of a reference instrument, which is the method AERONET uses to routinely calibrate its sun photometers.

3.2 Limitations of laboratory calibration

Hickey (1970) and Booth et al. (1994) found that the difference between the solar and lamp spectra is not negligible when working with moderate bandwidth radiometers (i.e. UV-MFRSR). A solution to this problem is introducing a calibration constant that references both the lamps and solar spectra (Booth et al., 1994). However, applying this method for routine network calibration requires the circulation of the field instrument to be collocated with the reference spectroradiometer for an adequate period while the gaps in the monitoring record at each site are minimized, which is hard to sustain (Bigelow et al., 1998). Alexandrov et al. (2009) emphasizes that

MFRSR filters may experience rapid sensitivity loss; i.e. Alexandrov et al. (2002) reported the loss of filter transmittance approximately by a factor of 3 for two MFRSR channels during the first 200 days of instrument operation, followed by gradual stabilization.

Augustine et al. (2003) pointed out that periodic calibration throughout the year is necessary because the extraterrestrial signal will slowly change due to filter drift.

4 In situ calibration

4.1 Langley method

The attenuation of the Sun's direct beam irradiance through the Earth's atmosphere can be described by the Bouguer-Lambert law (Beer's law):

$$I_\lambda = R^2 I_{0,\lambda} \exp(-\tau_{Total,\lambda} \cdot m), \tag{7}$$

where I_λ is the band-pass direct normal irradiance reaching surface at channel λ. R is the Earth-Sun distance in astronomical units (AU). $I_{0,\lambda} = \int I_{0,\lambda t} F_{\lambda t} \mathrm{d}\lambda_t / \int F_{\lambda t} \mathrm{d}\lambda_t$ is the band-pass extraterrestrial solar irradiance at channel λ, where $F_{\lambda t}$ is the filter function, or SRF, of the channel λ at wavelength λ_t and $I_{0,\lambda t}$ is the corresponding extraterrestrial solar irradiance.

There are many sources that provide $I_{0,\lambda t}$ of various spectral resolutions; one of them is the Atmospheric Laboratory for Applications and Science (ATLAS) mission with the Solar Spectral Irradiance Measurements (SOLSPEC) spectrometer (Thuillier et al., 1998). Molling et al. (2010) pointed out that $I_{0,\lambda}$ can change by as much as 0.2% over a few days, depending on sunspot activity. From 1978 to 2002, solar input at the top of atmosphere increased at a rate of 0.05% per decade (Willson and Mordvinov, 2003). Schmid et al. (1998) compared the uncertainty of several $I_{0,\lambda}$ and determined that since the uncertainty due to atmospheric conditions is at least one magnitude larger, it is acceptable that one considers $I_{0,\lambda}$ as a constant and known value for calibration.

The band-pass total optical depth at channel λ is $\tau_{Total,\lambda}$, and m is the airmass. In Slusser et al. (2000), Wilson and Forgan (1995), and Schmid and Wehrli (1995), the term $(\tau_{Total,\lambda})(m)$ is described as the sum of the optical depth of each scatterer or absorber and the corresponding airmass: $\sum_i (\tau_{i,\lambda})(m_i)$, where i indicates the ith scatterer or absorber. It is noted that m_i can vary slightly for different scatterers and absorbers (i.e. ozone, air molecules, and aerosols) due to their different altitude concentration profiles (Thomason et al., 1983). The airmass m is defined as the ratio of the path length of solar radiation incident at zenith angle z and the zenith path length. For solar zenith angles up to 75°, $m \approx 1/cos(z)$ is accurate enough. For higher solar zenith angles, more accurate approximation equations should be used (Kasten and Young, 1989).

For each MFRSR channel λ, the calibration factor can also be expressed as:

$$c_\lambda = V_{0,\lambda} / I_{0,\lambda}, \tag{8}$$

where, $V_{0,\lambda}$ is the corresponding voltage measured by the MFRSR as if it is deployed at the top of the atmosphere (airmass = 0). Applying Eqs. (8) and (6) to Eq. (7), we get

$$V_\lambda = R^2 V_{0,\lambda} \exp(-\tau_{Total,\lambda} \cdot m). \tag{9}$$

Taking the natural logarithm on both sides of Eq. (9),

$$\ln(V_\lambda / R^2) = \ln V_{0,\lambda} - \tau_{Total,\lambda} \cdot m. \tag{10}$$

For each direct beam measurement at channel λ, there are two unknown terms: $\ln V_{0,\lambda}$ and $\tau_{Total,\lambda}$. Generally, one equation with two unknowns does not have a definite solution. The Langley method introduces an additional constraint to solve these two unknown variables: the total optical depth is stable during the morning or afternoon calibration period. With this additional constraint, $\ln V_{0,\lambda}$ and $\tau_{Total,\lambda}$ may be solved simultaneously with a linear regression where $\ln V_{0,\lambda}$ is the intercept and $\tau_{Total,\lambda}$ is the negative of the slope. Note that cloudy measurements should be removed before one performs this linear regression. The subsection below will discuss the cloud screening methods.

4.1.1 Two corrections for UV Langley regression (Slusser et al., 2000)

For the visible channels, only the variation of aerosol optical depth may significantly affect the performance of the Langley regression. In UV channels, especially channels under 320 nm, the ozone cross section changes rapidly with wavelength. The finite band-pass correction factor is defined as the ratio of the surface direct beam irradiance at the wavelength of the peak of the filter function and the band-pass surface direct beam irradiance. Slusser et al. (2000) used the Tropospheric Ultraviolet & Visible Radiation Model (TUV) to calculate the irradiances for the finite band-pass correction factor. The TUV model uses parameters airmass range [1.2, 2.2] and total column ozone, 300 DU.

The other correction factor accounts for the difference between ozone airmass and the molecular airmass. Komhyr (1980) described the calculation details of ozone and molecular airmass. Instead of the correction factor, one can do the Langley regression using the reduced or weighted airmass, $m_{red} = \sum m_i \cdot \tau_i / \sum \tau_i$, described by Forgan (1988) to eliminate the airmass effects.

Janson and Slusser (2003) reported that the mean annual drifts in sensitivity for the seven nominal wavelengths of

the UV-MFRSR instrument are: 300 nm −0.9%, 305 nm −3.5%, 311 nm −3.5%, 317 nm −4.3%, 325 nm −3.8%, 332 nm −3.7%, 368 nm −3.5%.

4.1.2 The choice of airmass range

The reasons for limiting of airmass to a certain range include: (i) The uncertainty of the cosine angle correction and the shadow-band correction of MFRSR at high incident angles is increased (Mazzola et al., 2010; Alexandrov et al., 2004); (ii) High solar zenith angles have higher chances of cloud contamination due to a decreased probability gap for vertically developed clouds (Smirnov et al., 2000); (iii) Airmass near 1 usually indicates a higher probability of turbulent atmospheric conditions, which is not optimal for the AOD stability assumption of the Langley method.

This choice of airmass range is not unique. Mazzola et al. (2010) and Alexandrov et al. (2004) selected the 2.0 to 5.0 range; Harrison and Michalsky (1994) chose the 2.0 to 6.0 range; and Forgan (1994) used the 2.5 to 5.5 range.

4.1.3 Cloud screening

Beer's law requires that no clouds are in the path of the direct solar beam. Clouds can attenuate the direct solar irradiance, or, if near the solar disk, contribute to more diffuse solar radiation.

di Sarra et al. (2008) identified cloud-free periods using images from the Total Sky Imager, visual observations of the sky, and data from the broadband channel of the MFRSR.

It is possible for one to perform manual selection of data points presenting the clear sky and radiatively stable conditions (Augustine et al., 2003). Mazzola et al. (2010) pointed out that screening the cloudy points using the visual examination is time-consuming and cannot be applied routinely. Alexandrov et al. (2004) commented that the results of manual screening depended on the skill of the examiner.

The cloud screening module of the Langley Analyzer (LA) is a set of filters on the series of $\ln V$–airmass points. The following description is based on the interpolation of the C source code of the LA program. In the UVMRP version of LA, points with voltage less than 0.02 V are discarded. The user can specify the points that fall into permissible airmass ranges (i.e. [2.0, 6.0]). The rest points in the desired airmass ranges are referred to as the permissible points hereafter. The permissible points within a morning/afternoon are first sorted by airmass in ascending order. The detection of cloud periods is implemented by searching for segments with the beginning points where $\ln V$ starts to increase and the ending points where $\ln V$ starts to decrease again in that series. Additionally, concavity in the series is checked by setting thresholds on the slope of lnV. To test this algorithm for more than a half day, the algorithm should be applied to the data of each half day and the returned clear sky points combined into one vector.

The cloud screening algorithm developed by Long and Ackerman (2000) is originally designed for irradiance series provided by calibrated pyranometers, which are broadband radiometers with an effective 160° field of view centered on the zenith. The screening process is iterative, with each step involving four tests. The first test sets maximum and minimum limits of the airmass normalized downwelling total shortwave irradiance to eliminate obvious cloudy points. The second test sets maximum limits of the airmass normalized downwelling diffuse irradiance to eliminate haze or thin cloud points. The third test eliminates points that have a change of irradiance in a given time outside of a certain range. The fourth test checks the variation in the measurements by using a normalized diffuse ratio. The points that pass these four tests are tentatively clear-sky points and are used to adjust the threshold values for the next iteration. When two consecutive iteration steps return the same set of points, the iteration stops and those points are the final clear-sky points.

Augustine et al. (2003) applied the cloud screening algorithm of Long and Ackerman (2000) to the SURFRAD broadband solar data in a two month period. They used the determined clear-sky periods for Langley calibration of the 500 nm channel of the collocated MFRSR because they believed that the noise was reduced and a confident extrapolation to $\ln V_0$ by simple linear regression was feasible. The example (Fig. 3 in Augustine et al., 2003) shows that the regression line passes the majority of the screened points. Many MFRSR networks do not have broadband solar data to do the cloud screening, which limits its application to automatic calibration of MFRSR in those programs.

The cloud screening method of Mazzola et al. (2010) "renormalizes" AODs to a common range by: (i) 10 min AOD average is subtracted from each instantaneous AOD value; (ii) add the typical value of AOD (namely 0.2) to step 1 results; (iii) calculate the relative standard deviation of step 2 results over each 10 min period; (iv) label the points from step 3 with a value greater than 0.08 as cloudy points.

Smirnov et al. (2000) developed an automatic cloud screening algorithm on the time series of aerosol optical depth derived from calibrated sunphotometers of AERONET. First, the data quality is checked. The points with negative values of AOD (< -0.01) or values lower than the stratospheric background AOD (Shaw, 1982) (varying with wavelength) are identified as cloudy or poor quality. Second, the triplet stability criterion is applied. The three measurements, each made 30 s apart, constitute a triplet. The points with AOD range in a triplet exceeding

Max{0.02, 0.03*AOD} are identified as cloudy. The empirical threshold value for any wavelength is 0.02 when AOD is lower than 0.7. When the AOD level is high (>0.7, indicating biomass burning or extremely hazy conditions, etc.), the threshold value is relaxed to be 0.03*AOD. Third, the diurnal stability is checked. The points with a standard deviation of AOD at 500 nm (or 440 nm) for the entire day that is larger than 0.015 are identified as cloudy. Fourth, the smoothness criteria are applied. It is assumed that the second derivative of the time series of optical depth is very sensitive to that caused by nearby cloudy points. To ensure a coherent threshold value, they designed the logarithmic second derivative (D) of optical depth:

$$D=\sqrt{\frac{1}{(n-2)}\sum\left[\frac{\ln\ \tau_i-\ln\ \tau_{i+1}}{t_i-t_{i+1}}-\frac{\ln\ \tau_{i+1}-\ln\ \tau_{i+2}}{t_{i+1}-t_{i+2}}\right]^2}. \tag{11}$$

They recursively removed the points with maximum optical depth until $D\leqslant 16$. Then they applied the diurnal stability check again and repeated the third and fourth steps until no elimination occurred. Fifth, the 3-σ criterion is applied. Any points that are outside of the 3-σ range of the mean AOD at 500 nm or Angstrom coefficient α (440–870 nm) are identified as cloudy.

Based on the variability analysis of derived optical depth, Alexandrov et al. (2004) developed an automated cloud screening algorithm using single channel direct beam measurements of a VIS-MFRSR. Their algorithm is based on the inhomogeneity parameter (ε) (Cahalan, 1994; Cairns et al., 2000):

$$\varepsilon=1-\frac{\exp(\overline{\ln\ \tau})}{\overline{\tau}}, \tag{12}$$

where the over-line refers to averaging over time. The inhomogeneity parameter, ε, can vary from 0 for completely homogeneous to 1 for extremely inhomogeneous air conditions. To better separate aerosols and some types of clouds (thin cirrus, marine boundary layer clouds), ε is modified as:

$$\varepsilon'=1-\frac{\exp(\overline{\ln\ \tau'})}{\overline{\tau'}}, \tag{13}$$

where $\tau'=\tau-\overline{\tau}+\tau_{const}$ is the renormalized optical depth. The statistical distribution of values of the inhomogeneity parameter ε′ over a month shows two distinctive maxima that correspond to the aerosol and cloud modes respectively. Aerosols have a lower ε′ than clouds. The threshold value of ε′ between the two modes is 2×10^{-4}, below which are considered clear and above which are considered cloudy. It is noted that this approach can misidentify a very short clear sky interval between clouds as being cloudy, although the probability of this situation is small.

4.1.4 Reasons for the failure of the Langley method (summarized by Augustine et al., 2003)

(1) A change in aerosol optical depth over the course of a calibration period. The assumption of AOD stability is critical to the Langley method, for which Forgan (1986) made a sensitivity analysis: A change in aerosol optical depth of 0.003 will produce an error of about 1 percent in the calibration coefficient. For a 368 nm channel, a change of absolute aerosol optical depth at 0.003 represents less than 0.6% change in optical depth. But the observed percent change of a typical sea-level station is between 3% and 10%. Wilson and Forgan (1995) mentioned methods to overcome the limitations that are due to atmospheric variability; all involve information that is not commonly available for a long-term operational MFRSR such as deployment of another calibrated instrument or knowing calibration information in a certain channel.

(2) Effects of atmospheric noise such as that from subvisual cirrus (Shaw, 1976). Thin clouds may have optical depth as low as aerosols. However, Beer's law is not valid for cloudy conditions, which means including such points in a Langley regression may significantly bias the regression intercept ($\ln V_0$).

(3) Instrument errors. This covers some complicated situations. For example, the internal temperature of the MFRSR is supposed to be maintained constantly at around 40°C or 42°C; however, in summer at some southern sites, the actual internal temperature can be 10°C higher than the defined constant near noon. The diurnal variation of voltages due to this factor can result in a biased intercept ($\ln V_0$). Alexandrov et al. (2007) mentioned that the precision of instrument alignment should be considered. The AOD errors induced by a 1° tilt are on the order of 0.01.

(4) Harrison et al. (1994b) report that the relatively large field of view of an MFRSR makes it vulnerable to the adverse effects of enhanced forward scattering by aerosols or thin cirrus cloud particles whose dimensions are large compared to the wavelength of the measurement. These enhanced signals artificially decrease the inferred total optical depth.

4.1.5 Two variants of Langley method

On-site calibration technique: Krotkov et al. (2005) calculate V_0 (325, 332, and 368 nm channels) of UV-MFRSR using Beer's law with all components of optical depth prepared before calibration. Total column ozone is obtained from climatological mean ozone values, aerosol optical depth is extrapolated/interpolated in both wavelength and temporal dimensions from AERONET-CIMEL measurements, and Rayleigh optical depth is calculated using the method by Bodhaine et al. (1999). Extraterrestrial spectral solar irradiance is taken from

SUSIM AtLAS-3 measurements. There is only one unknown variable in Eq. (10): V_0, which can be calculated for each time point. The daily mean V_0 is calculated by iteratively removing points outside of three times the standard deviation. The stability of this method is about±2% in summer and larger in fall-winter seasons. This method requires accurate aerosol optical depth availability before calibration, which limits its application in most MFRSR sites.

The main modification Lee et al. (2010) proposed to the standard Langley method involves the acquisition of the maximum value composite (MVC) of the largest irradiance (voltage) values during a several day window in each small airmass interval. The abnormal values are eliminated by applying a threshold on the standard deviation of relative difference in each bin. The window sizes vary from 5 to 30 days. The comparison of the derived AOD using this method to the interpolated AOD of AERONET showed that the relative error of AOD for 5, 7, and 10 days are about 20% and equal to 7.5% for 30 days.

4.2 Ratio-Langley method (Forgan, 1986)

Forgan (1986) pointed out that the variation of aerosol optical depth by changes of particle number, the aerosol size distribution, or both, affects all channels at different degrees depending on the optical efficiency as a function of particle size and wavelength.

In the two channels (λ_1 and λ_2) where gaseous absorption is negligible or constant with time, the difference of total optical depth between them ($\tau_1(t)-\tau_2(t)$) is the combination of a constant (dominated by molecular scattering and absorption) and a varying term caused by aerosols. Dividing the Beer's Law equations at λ_1 and λ_2, and taking a logarithm on both sides, one gets the following equation:

$$\ln\left(\frac{V_1(t)}{V_2(t)}\right) = \ln\left(\frac{V_{01}}{V_{02}}\right) - \left(\tau_1(t)-\tau_2(t)\right)\cdot m(t). \quad (14)$$

Sensitivity analysis on the Angstrom exponential formula shows that for aerosol distributions dominated by large particles (i.e. marine environments), $|\tau_{a1}(t)-\tau_{a2}(t)|\rightarrow 0$, which suggests that a Langley-like regression on Eq. (14) will give a more accurate and stable intercept term V_{01}/V_{02}.

Strictly speaking, the ratio-Langley method alone cannot provide calibration coefficients for any individual channel. Instead, it provides the ratio of calibration coefficients at two channels (V_{01}/V_{02}). If the calibration coefficient at one channel is determined by other means, all calibration coefficients can be calculated using the ratio results.

4.3 General method (Forgan, 1994)

The fundamental assumptions of the general method are that the relative size distribution f is dependent only on particle radius r and the multiplier A is only a function of time t. With these assumptions, the aerosol size distribution can be expressed as $\partial N(t)/\partial \ln r = A(t)f(r)$. The aerosol optical depth (τ_a) for this distribution at time t and wavelength λ is given by

$$\tau_a(t,\lambda) = \pi A(t)\int Q_{ext}(r,\lambda)r^2 f(r)\mathrm{d}\ln r, \quad (15)$$

where Q_{ext} is the extinction efficiency, which is a function of the wavelength and the particle radius. It is seen that the only term in this expression that is dependent on time is the multiplier A. Therefore, the optical depth at any time t can be related to that at the reference time t_0, $\tau_a(t,\lambda) = \tau_a(t_0,\lambda)A(t)/A(t_0)$. The ratio of optical depths at any time t between two wavelengths (λ_0 and λ_1) is a constant (defined as ψ_{01}):

$$\begin{aligned}\frac{\tau_a(t,\lambda_1)}{\tau_a(t,\lambda_0)} &= \frac{\tau_a(t_0,\lambda_1)A(t)/A(t_0)}{\tau_a(t_0,\lambda_0)A(t)/A(t_0)} \\ &= \frac{\tau_a(t_0,\lambda_1)}{\tau_a(t_0,\lambda_0)} = \mathrm{constant}\, t = \psi_{01}\end{aligned} \quad (16)$$

for all t.

If the Beer-Lambert's law is valid on both wavelengths, one can derive the logarithm of the calibration factor of the target wavelength ($-\ln V_{0\_1}$) and the constant (ψ_{01}) through a least squares regression on the following expression:

$$\begin{aligned}&\{-[\ln V_1(t) + m_m(t)\tau_m(t,\lambda_1) + m_g\tau_g(t,\lambda_1)]\} \\ &= \psi_{01}[m_a(t)\tau_a(t,\lambda_0)] + \{-\ln V_{0\_1}\}.\end{aligned} \quad (17)$$

The three terms on the left side of the equal sign are measurements ($V_1(t)$) or calculable values (airmass, molecular scattering, and absorption optical depths). There are two ways of providing the aerosol optical depth at the other wavelength $[m_a(t)\tau_a(t,\lambda_0)]$: (i) using a well-calibrated sun photometer; or (ii) using solar Aureole Measurements (Forgan, 1987).

4.4 Comprehensive calibration method with atmospheric quantities retrieval (Alexandrov et al., 2002)

This method provides for the simultaneous determination of the instrument's calibration coefficients together with the retrieval of physical quantities. This method is designed for 5 channels (415–870 nm) of VIS-MFRSR. The basic equation used is Beer's law. The major improvement of this method is that it relaxes the strong assumption of stability of aerosol optical depth to that of aerosol spectral extinction properties during the calibration period (determined by composition and particle size distribution). This method does not require any additional measurements from other instruments. Depending on the

wavelength, the significant components of the total optical depth may include Rayleigh, aerosol, nitrogen dioxide, and ozone. There are several methods for approximating the Rayleigh optical depth with comparable results (Hansen and Travis, 1974; Bucholtz, 1995; Bodhaine et al., 1999). They remove it to get the adjusted total optical depth. They manually select clear-sky points. There are four main steps of this method:

(1) The first step of the retrieval algorithm is the determination of the 870 nm optical depth and calibration coefficient.

The reason for the choice of 870 nm channel is that diffuse flux is only affected by aerosols, which means the vertical distribution of gaseous absorbers (nitrogen dioxide and ozone) can be unknown.

The direct to diffuse irradiance ratio from the same MFRSR is independent of instrumental calibration. Therefore, the difference between the optical depth derived from the uncalibrated direct beam measurement and that inverted from the calibration-independent ratio of the direct and diffuse intensities (voltages) is considered the calibration effect. Some factors cause the discrepancy between the two even with the calibration effect considered. They overcome this issue by using observed stability (over several months) of the missing opacity.

They first assume an initial asymmetry parameter of 0.75 then determine the actual particle size, and then rerun the calibration routine with the new asymmetry parameter thereby iteratively correcting the calibration coefficient.

The retrieval of optical depth from direct-diffuse ratio relies on the simplified analytical relationship:

$$A = \frac{1}{R}\left(\frac{1-(\Phi/\Phi_0)}{1+\Phi\cdot\cos\theta}\right), \tag{18}$$

where A is the surface albedo; $\Phi = I_{dir}/I_{dif} = V_{dir}/V_{dif}$ is the corresponding direct-diffuse ratio; and Φ_0 is the zero surface reflectivity. The scattering angle integrated reflection function, R, can be seen as an implicit function of optical depth. The retrieved aerosol optical depth depends only weakly on surface albedo, so although the surface albedo is an unknown quantity, a reasonable assumption of $0 < A < 50\%$ results in the uncertainty of ± 0.01 in the optical depth inverted from Eq. (18). This calibration procedure works well even for days with highly variable optical depth.

(2) The second step is an analytical solution of a set of linear equations to retrieve the aerosol optical depths for all five channels.

The assumption is that the aerosol spectral extinction Q^i_{ext} is more stable while the aerosol optical depth is changing systematically during the day. Starting from Beer's law, they define the un-calibrated optical depth for the ith channel as

$$\widetilde{\tau}_i = -\mu\cdot\ln\frac{V_i}{V_0} = \tau_i + s_i\cdot\mu, \tag{19}$$

where $s_i = -\ln c_i$ and c_i is the calibration coefficient for channel i; $\tau_i = q_i\tau_a + \beta_i x_{NO_2} + \gamma_i x_{O_3}$ is the total optical depth for channel i; $q_i = Q^i_{ext}/Q^5_{ext}$ is the Mie-scattering extinction ratio normalized to the fifth (870 nm) channel: By definition, q_5 is equal to 1, all other q_i are unknown but assumed to be invariant over the calibration period; τ_a is the aerosol optical depth of channel 5; β_i and γ_i are the effective spectral absorption coefficients for nitrogen dioxide and ozone, respectively, for channel i: $\gamma_1 = 0$, $\gamma_5 = 0$, $\beta_5 = 0$, all others are measured values from previous studies; x_{NO_2} and x_{O_3} are the column nitrogen dioxide and column ozone in Dobson units, respectively; and μ is the cosine of the solar zenith angle. From step (1), one already has s_5 and τ_a. Substituting them into Eq. (19) for the rest of the channels and dividing the expressions by μ, they obtain the following equations:

$$\begin{aligned} F_3 &= B_3(x - s_5) + A_3, \\ F_4 &= B_4(x - s_5) + A_4, \end{aligned} \tag{20}$$

where

$$x = \mu^{-1}\cdot\widetilde{\tau}_5, \tag{21}$$

$$F_i = \mu^{-1}[\widetilde{\tau}_i - b_{i1}\widetilde{\tau}_1 - g_{i2}(\widetilde{\tau}_2 - b_{21}\widetilde{\tau}_1)], \tag{22}$$

$$B_i = q_i - b_{i1}q_1 - g_{i2}(q_2 - b_{21}q_1), \tag{23}$$

$$A_i = s_i - b_{i1}s_1 - g_{i2}(s_2 - b_{21}s_1). \tag{24}$$

And where $i \in [3,4]$; $b_{ij} = \beta_i/\beta_j$ and $g_{ij} = \gamma_i/\gamma_j$ are the spectrally weighted nitrogen dioxide and ozone absorption coefficient ratios, which can be treated as known values, respectively. In Eq. (20), the calculation of the left-hand side, Eq. (22), at each time step only involves measurements and known values. On the right-hand side, x and s_5 are measurements and retrieved value; both B_i and A_i are unknown but constant over the calibration period since the calibration factors s_i and the aerosol extinction ratios q_i are expected to be constant over the period. Therefore, one can retrieve the unknowns (B_3, B_4, A_3, and A_4) in Eq. (20) with a linear regression similar to Langley regression.

The two aerosol size distribution parameters, the effective radius r_{eff} and the effective variance v_{eff}, are used to build a look-up table for B_3 and B_4 via Eq. (23) and Mie theory. The combination of r_{eff} and v_{eff} that matches the regression results of B_3 and B_4 are the solutions. To reduce the influence of error in measurements and calibrations, they limit $v_{eff} = 0.01$ to average out the oscillations and the corresponding r_{eff} is referred to as "monodistribution radius." Now only B_3 is needed to retrieve r_{eff}, which is considered to generate more stable result than B_4. Once r_{eff} is determined, the aerosol optical depth, at any wavelength, can be calculated from the Mie spectral extinction parameter and τ_a (the aerosol optical depth at 870 nm obtained in step (1)).

(3) The third step is the retrieval of the nitrogen dioxide and ozone column amounts, as well as the first two channel calibration coefficients.

The aerosol optical depths retrieved from step (2) are removed from Eq. (19). Since $\gamma_1 = 0$, the unknown optical depth left for channel 1 (415 nm) is due to nitrogen dioxide. Assuming the stability of nitrogen dioxide over the calibration period, one can perform a Langley-like regression to solve s_1 and the average column nitrogen dioxide (x_{NO_2}) together.

By removing the aerosol and nitrogen dioxide optical depth from Eq. (19), one can perform a Langley-like regression on channel 2 to solve s_2 and the column ozone (x_{O_3}) together.

(4) The fourth step is the determination of the calibration coefficients for the rest of the channels.

The last two calibration coefficients, s_3 and s_4, can be calculated using Eq. (24); s_1 and s_2 are retrieved in step (3).

4.5 Nonlinear optimization with Bi-channel Langley and Angstrom law constraints

The calibration method of Chen et al. (2012) relies on two essential constraints: (π) the AOD difference between channels is constant over time, which is fulfilled by the bi-channel Langley method; and (θ) the AOD ratio between channels is constant over time, which is implemented by the Angstrom law. The technique "bi-channel Langley method" is similar to the "ratio-Langley method" described in the previous section. These constraints are applied in two consecutive optimization steps to solve the calibration factors (V_0) and AOD in the target channels using the trust region based nonlinear optimization module called CONDOR (Vanden Berghen and Bersini, 2005). Two channels are the minimum requirement for this method, while multiple channels in the 368 to 870 nm range can be solved simultaneously with this method. The example shows better agreement of AOD derived from this method than that of the standard Langley method to the collocated AERONET AOD, which implies improvement in the retrieved calibration factors. Note that Angstrom law is empirical and may not be suitable for some cases, which limits its application.

4.6 Water vapor channel calibration

Alexandrov et al. (2009) reviewed the papers that describe the retrieval of precipitable water vapor (and determination of calibration factors in some papers) using ground based radiometers at 940 nm channel: Fowle (1912, 1915), Reagan et al. (1987a, 1987b, 1995), Bruegge et al. (1992), Thome et al. (1992, 1994), Michalsky et al. (1995b, 2001b), Schmid et al. (1996, 2001, 2003), Shiobara et al. (1996), Halthore et al. (1997), Cachorro et al. (1998), Plana-Fattori et al. (1998, 2004), Ingold et al. (2000), Kiedron et al. (2001, 2003), Livingston et al. (2007).

The calibration methods for the 940 nm channel can be characterized by the "Modified Langley plot" fitting technique (Reagan et al., 1987a, 1987b; Bruegge et al., 1992).

The transmission of water vapor (T_{water}) is modeled as a function of the water vapor column (u),

$$T_{water} = \exp\left(-k \cdot (m \cdot u)^b\right), \tag{25}$$

where k and b are constants for a particular filter. For the purpose of determining k and b, m is set to 1. Rearranging the terms,

$$\ln\left(\ln\left(1/T_{water}\right)\right) = \ln k + b \cdot \ln u. \tag{26}$$

One can calculate the effective transmission of water vapor (convolution of the normalized SRF and the atmospheric transmission of water vapor over wavelength of the filter pass-band) as a function of u using LOWTRAN7. Once the expected range of u is covered, one can perform a least squares fit to Eq. (26) to obtain k and b for the particular filter/instrument.

Beer's law for the 940 nm channel considers the water vapor absorption,

$$V_{940} = R^2 V_{0,940} \exp\Big(-(\tau_{aerosol,940} + \tau_{Rayleigh,940}) \cdot m\Big) \cdot T_{water}. \tag{27}$$

Taking the natural logarithm of Eq. (27) and rearranging it,

$$\ln\left(V_{940}/R^2\right) + (\tau_{aerosol,940} + \tau_{Rayleigh,940}) \cdot m = \ln V_{0,940} - (k \cdot m^b) \cdot u^b. \tag{28}$$

The calculation of $\tau_{Rayleigh}$ at any given wavelength has been discussed (Bodhaine et al., 1999). The value of $\tau_{aerosol,940}$ can be estimated by extrapolating on the $\log \tau_{aerosol} - \log \lambda$ plot. Similar to the Langley method, assuming the water vapor column remains constant in the calibration period, one can perform a linear regression on Eq. (28) to determine the intercept, $\ln(V_{0,940})$, and the slope, u^b, simultaneously.

Alexandrov et al. (2009) found that the fundamental assumption of this technique: the stability of the precipitable water vapor (PWV) column, which is similar to that of the standard Langley method, rarely occurs in reality, except for very dry sites like the Arctic (Kiedron et al., 2001) or high mountains (Schmid et al., 1998). In other cases this technique cannot provide accurate calibration factors or PWV with low uncertainty (Michalsky et al., 2001b). Because of this, research that involves a 940 nm

channel usually uses lamp calibration instead of this technique (Alexandrov et al., 2009; Hodges and Michalsky, 2011).

5 Conclusions

The MFRSR, both the visible and ultraviolet versions, is a widely deployed radiometer that has measured surface shortwave radiation with high sampling rate for about two decades. It has been used for validating satellite observation and retrievals and for monitoring important properties of gases, aerosols, and clouds in the atmosphere. Except for the parameters that can be derived from the ratio of its measured components, which are not impacted by calibration error, most applications require accurate calibration factors, angular correction, and spectral response functions provided by calibration. Although the laboratory lamp, or reference, calibration can provide all the information needed to convert the readings to actual radiation, in situ calibration methods are implemented routinely to fill the gaps between lamp calibrations. In situ calibration with collocated AOD measurements can provide accurate calibration factors. However, information of AOD is not available for most deployed MFRSR units, which limits its application. In situ calibration methods based on Beer's law with no ancillary AOD measurements are fundamentally underdetermined problems. They assume some properties, such as AOD, TOD, precipitable water vapor, effective size of aerosol particles, and angstrom coefficient, are invariant over time in order to create equations solvable by linear regression or nonlinear optimization. Since these artificial assumptions are not universal and some of them rarely happen, there is no single in situ calibration method that is suitable for all sites at all times. In practice, daily calibration factors derived from these methods should be time-smoothed with or without lamp calibration information to restrain error.

Acknowledgements This work is supported by USDA UVB Monitoring and Research Program under Grant No. USDA NIFA project (2011-34263-30654).

References

Ackerman T P, Stokes G (2003). The atmospheric radiation measurement program. Phys Today, 56(1): 38–45

Alexandrov, D, Kiedron P, Michalsky J J, Godges G, Flynn C J, Lacis A A (2007). Optical depth measurements by shadow-band radiometers and their uncertainties. Appl Opt, 46(33): 8027–8038

Alexandrov M D, Lacis A A, Carlson B E, Cairns B (2002). Remote sensing of atmospheric aerosols and trace gases by means of multifilter rotating shadowband radiometer. part I: retrieval algorithm. J Atmos Sci, 59(3): 524–543

Alexandrov M D, Lacis A A, Carlson B E, Cairns B (2002b). Remote sensing of atmospheric aerosols and trace gases by means of multifilter rotating shadowband radiometer. part II: climatological applications. J Atmos Sci, 59(3): 544–566

Alexandrov M D, Lacis A A, Carlson B E, Cairns B (2008). Characterization of atmospheric aerosols using MFRSR measurements. J Geophys Res, 113(D8): D08204

Alexandrov M D, Marshak A, Cairns B, Lacis A A, Carlson B E (2004). Automated cloud screening algorithm for MFRSR data. Geophys Res Lett, 31(4): L04118

Alexandrov M D, Schmid B, Turner D D, Cairns B, Oinas V, Lacis A A, Gutman S I, Westwater E R, Smirnov A, Eilers J (2009). Columnar water vapor retrievals from multifilter rotating shadowband radiometer data. J Geophys Res, 114(D2): D02306

Augustine J A, Cornwall C R, Hodges G B, Long C N, Medina C I, DeLuisi J J (2003). An automated method of MFRSR calibration for aerosol optical depth analysis with application to an Asian dust outbreak over the United States. J Appl Meteorol, 42(2): 266–278

Augustine J A, Hodges G B, Cornwall C R, Michalsky J J, Medina C I (2005). An update on SURFRAD – The GCOS Surface Radiation budget network for the continental United States. J Atmos Ocean Technol, 22(10): 1460–1472

Bais A F (1997). Spectrometers: operational errors and uncertainties, Solar Ultraviolet Radiation Modeling, Measurements and Effects. In: Zerefos C S, Bais A F, eds .Vol. 52 of NATO ASI Series I, Global Environmental Change. Berlin: Springer-Verlag, 163–173

Bais A F, Kazadzis S, Balis D, Zerefos C S, Blumthaler M (1998). Correcting global solar ultraviolet spectra recorded by a brewer spectroradiometer for its angular response error. Appl Opt, 37(27): 6339–6344

Bigelow D S, Slusser J R, Beaubien A F, Gibson J H (1998). The USDA ultraviolet radiation monitoring program. Bull Am Meteorol Soc, 79 (4): 601–615

Blumthaler M, Bais A F (1996). Cosine corrections of global sky measurements, In: Kjeldstad B, Johnsen B, Koskela T, eds. The Nordic Intercomparison of Ultraviolet and Total Ozone Instruments at Izana October 1996. Helsinki: Finnish Meteorological Institute, 161–172

Bodhaine B A, Wood N B, Dutton E G, Slusser J R (1999). On Rayleigh optical depth calculations. J Atmos Oceanic Technol, 16: 1854–1861

Booth C R, Mestechkina T, Morrow J H (1994). Errors in the reporting of solar spectral irradiance using moderate bandwidth radiometers: an experimental investigation. In: Ocean Optics XII, Proc SPIE Int Soc Opt Eng, 2258, 654–663

Bruegge C J, Conel J E, Green R O, Margolis J S, Holm R G, Toon G (1992). Water vapor column abundance retrievals during FTFE. J Geophys Res, 97(D17): 18759–18768

Bucholtz A (1995). Rayleigh-scattering calculations for the terrestrial atmosphere. Appl Opt, 34(15): 6339–6344

Cachorro V E, Utrillas P, Vergaz R, Duran P, de Frutos A M, Martinez-Lozano J A (1998). Determination of the atmospheric water-vapor content in the 940-nm absorption band by use of moderate spectral-resolution measurements of direct solar irradiance. Appl Opt, 37(21): 4678–4689

Cahalan R F (1994). Bounded cascade clouds: Albedo and effective thickness. Nonlinear Process Geophys, 1(2/3): 156–167

Cairns B, Lacis A A, Carlson B E (2000). Absorption within inhomogeneous clouds and its parameterization in general circulation models. J Atmos Sci, 57(5): 700–714

Caldwell M M, Camp C W, Warner C W, Flint S D (1986). Action spectra and their role in assessing biological consequences of solar UV-B radiation change. In: Worrest R C, Caldwell M M, eds. Stratospheric Ozone Reduction, Solar Ultraviolet Radiation and Plant Life. Berlin: Springer-Verlag, 87–111

Charlson R J, Schwartz S E, Hales J M, Cess R D, Coakley J A Jr, Hansen J E, Hofmann D J (1992). Climate forcing by anthropogenic aerosols. Science. New Series, 255(5043): 423–430

Chen M, Davis J, Tang H, Gao Z, Gao W (2012). A multi-channel calibration method for multi-filter rotating shadow-band radiometer. Proc SPIE 8513. Remote Sensing and Modeling of Ecosystems for Sustainability, IX: 851305

Chow J C, Watson J G, Fujita E M, Lu Z, Lawson D R (1994). Temporal and spatial variations of $PM_{2.5}$ and PM_{10} aerosol in the Southern California air quality study. Atmospheric Environment, 28(12): 2061–2080

di Sarra A, Fua D, Cacciani M, Di Iorio T, Disterhoft P, Meloni D, Monteleone F, Piacentino S, Sferlazzo D (2008). Determination of ultraviolet cosine-corrected irradiances and aerosol optical thickness by combined measurements with a Brewer spectrophotometer and a multifilter rotating shadowband radiometer. Appl Opt, 47(33): 6142–6150

Feister U, Grewe R, Gericke K (1997). A method for correction of cosine errors in measurements of spectral UV irradiance. Sol Energy, 60(6): 313–332

Forgan B W (1986). Sun photometer calibration by the ratio-Langley technique. In: Forgan B W, Fraser P J, eds. Baseline Atmospheric Program, Bureau of Meteorology, Melbourne, Australia, 22–26

Forgan B W (1987). A technique for calibrating sunphotometers using solar aureole measurements. In: Forgan B W, Ayers G P, eds. Baseline, Bureau of Meteorology, Melbourne, Australia, 1989, 15–20

Forgan B W (1988). Bias in solar constant determination by the Langley method due to structured aerosol: Comment. Appl Opt, 27(12): 2546–2548

Forgan B W (1994). General method for calibrating Sun photometers. Appl Opt, 33(21): 4841–4850

Fowle F E (1912). The spectroscopic determination of aqueous vapor. Astrophys J, 35(3): 149–162

Fowle F E (1915). The transparency of aqueous vapor. Astrophys J, 42 (5): 394–411

Halthore R N, Eck T F, Holben B N, Markham B L (1997). Sun photometric measurements of atmospheric water vapor column abundance in the 940-nm band. J Geophys Res, 102(D4): 4343–4352

Hansen J E, Travis L D (1974). Light scattering in planetary atmospheres. Space Sci Rev, 16(4): 527–610

Harrison L, Michalsky J (1994). Objective algorithms for the retrieval of optical depths from ground-based measurements. Appl Opt, 33(22): 5126–5132

Harrison L, Michalsky J, Berndt J (1994b). Automated multifilter rotating shadow-band radiometer: an instrument for optical depth and radiation measurements. Appl Opt, 33(22): 5118–5125

Hickey J R (1970). Laboratory methods of experimental radiometry including data analysis. Adv Geophys, 14: 227–267

Hodges G B, Michalsky J J (2011). Multifilter Rotating Shadowband Radiometer (MFRSR) Handbook with Subsections for the Following Derivative Instruments: Multifilter Radiometer (MFR) Normal Incidence Multifilter Radiometer (NIMFR), U.S. Department of Energy, Office of Science, Office of Biological and Environmental Research, DOE/SC-ARM/TR-059

Holben B N, Eck T F, Slutsker I, Tanré D, Buis J P, Setzer A, Vermote E, Reagan J A, Kaufman Y J, Nakajima T, Lavenu F, Jankowiak I, Smirnov A (1998). AERONET–A federated instrument network and data archive for aerosol characterization. Remote Sens Environ, 66 (1): 1–16

Ingold T, Schmid B, Matzler C, Demoulin P, Kampfer N (2000). Modeled and empirical approaches for retrieving columnar water vapor from solar transmittance measurements in the 0.72, 0.82, and 0.94 mm absorption bands. J Geophys Res, 105(D19): 24327–24343

Janson G T, Slusser J R (2003). Long-term stability of UV multifilter rotating shadowband radiometers. Ultraviolet ground- and space-based measurements, Models and Effects III Book Series: Proceedings of the Society of Photo-Optical Instrumentation Engineers (SPIE), 5156: 94–100

Kakani V G, Reddy K R, Zhao D, Mohammed A R (2003b). Effects of ultraviolet-B radiation on cotton (*Gossypium hirsutum* L.) morphology and anatomy. Ann Bot (Lond), 91(7): 817–826

Kakani V G, Reddy K R, Zhao D, Sailaja K (2003a). Field crop responses to ultraviolet-B radiation: a review. Agric Meteorol, 120 (1–4): 191–218

Kaskaoutis D G, Kambezidis H D, Kharol S K, Badarinath K V S (2008). The diffuse-to-global spectral irradiance ratio as a cloud-screening technique for radiometric data. J Atmos Solar-Terrestrial Phys, 70 (13): 1597–1606

Kassianov E, Barnard J C, Berg L K, Flynn C, Long C N (2011). Sky cover from MFRSR observations. Atmos Meas Tech, 4: 1463–1470

Kasten F, Young A T (1989). Revised optical air mass tables and approximation formula. Appl Opt, 28(22): 4735–4738

Kiedron P, Berndt J, Michalsky J, Harrison L (2003). Column water vapor from diffuse irradiance. Geophys Res Lett, 30(11): 1565–1568

Kiedron P, Michalsky J, Schmid B, Slater D, Berndt J, Harrison L, Racette P, Westwater E, Han Y (2001). A robust retrieval of water vapor column in dry Arctic conditions using the rotating shadowband spectroradiometer. J Geophys Res, 106(D20): 24007–24016

Kiedron P W, Michalsky J J, Berndt J L, Harrison L C (1999). Comparison of spectral irradiance standards used to calibrate shortwave radiometers and spectroradiometers. Appl Opt, 38(12): 2432–2439

Komhyr W D (1980). Operations Handbook–Ozone Observations with a Dobson Spectrophotometer, WMO Global Ozone Res. Monit. Proj. Report 6, World Meteorol. Organ. Geneva

Krotkov N, Bhartia P K, Herman J, Slusser J, Labow G, Scott G, Janson G, Eck T F, Holben B (2005). Aerosol ultraviolet absorption experiment (2002 to 2004), part 1: ultraviolet multifilter rotating shadowband radiometer calibration and intercomparison with CIMEL sunphotometers. Opt Eng, 44(4): 041004

Lee K H, Li Z, Cribb M C, Liu J, Wang L, Zheng Y, Xia X, Chen H, Li B (2010). Aerosol optical depth measurements in eastern China and a new calibration method. J Geophys Res, 115: D00K11

Leontieva E, Stamnes K(1996). Remote sensing of cloud optical

properties from ground-based measurements of transmittance: a feasibility study. J Appl Meteor, 35(11): 2011–2022

Lighty J S, Veranth J M, Sarofim A F (2000). Combustion aerosols: factors governing their size and composition and implications to human health. J Air Waste Manag Assoc, 50(9): 1565–1618

Livingston J, Schmid B, Redemann J, Russell P B, Ramirez S A, Eilers J, Gore W, Howard S, Pommier J, Fetzer E J, Seemann S W, Borbas E, Wolfe D E, Thompson A M (2007). Comparison of water vapor measurements by airborne Sun photometer and near-coincident in situ and satellite sensors during INTEX/ITCT 2004. J Geophys Res, 112(D12): D12S16

Long C N, Ackerman T P (2000). Identification of clear skies from broadband pyranometer measurements and calculation of downwelling shortwave cloud effects. J Geophys Res, 105(D12): 15609–15626

Madronich S (1993). UV radiation in the natural and perturbed atmosphere. In: Tevini M, ed., UV-B Radiation and Ozone Depletion: Effects on Humans, Animals, Plants, Microorganisms, and Materials. Boca Raton: Lewis Publishers

Mazzola M, Lanconelli C, Lupi A, Busetto M, Vitale V, Tomasi C (2010). Columnar aerosol optical properties in the Po Valley, Italy, from MFRSR data. J Geophys Res, 115(D17): D17206

Michalsky J J, Harrison L C, Berkheiser W E III (1995). Cosine response characteristics of some radiometric and photometric sensors. Sol Energy, 54(6): 397–402

Michalsky J J, Liljegren J C, Harrison L C (1995b). A comparison of Sun photometer derivations of total column water vapor and ozone to standard measures of same at the Southern Great Plains Atmospheric Radiation Measurement site. J Geophys Res, 100(D12): 25,995–26,003

Michalsky J J, Min Q, Kiedron P W, Slater D W, Barnard J C (2001b). A differential technique to retrieve column water vapor using sun radiometry. J Geophys Res, 106(D15): 17,433–17,442

Michalsky J J, Schlemmer F A, Berkheiser W E, Berndt J L, Harrison L C, Laulainen N S, Larson N R, Barnard J C (2001a). Multi-year measurements of aerosol optical depth in the Atmospheric Radiation Measurement and Quantitative Links programs. J Geophys Res, 106 (D11): 12099–12107

Molling C C, Heidinger A K, Straka W C III and Wu X (2010). Calibrations for AVHRR channels 1 and 2: review and path towards consensus. International Journal of Remote Sensing, 31(24): 6519–6540

Monteith J L, Unsworth M H (2008), Principles of environmental physics, 3rd ed. Oxford: Academic

Plana-Fattori A, Dubuisson P, Fomin B A, de Paula Corrêa M (2004). Estimating the atmospheric water vapor content from multi-filter rotating shadow-band radiometry at Sao Paulo, Brazil. Atmos Res, 71 (3): 171–192

Plana-Fattori A, Legrand M, Tanre D, Devaux C, Vermeulen A, Dubuisson P (1998). Estimating the atmospheric water vapor content from Sun photometer measurements. J Appl Meteorol, 37(8): 790–804

Ramanathan V, Cess R D, Harrison E F, Minnis P, Barkstrom B R, Ahmad E, Hartmann D (1989). Cloud-radiative forcing and climate: results from the Earth radiation budget experiment. Science, 243 (4887): 57–63

Ramanathan V, Crutzen P J, Kiehl J T, Rosenfeld D (2001). Aerosols, climate, and the hydrological cycle. Science, 294(5549): 2119–2124

Reagan J, Thome K, Herman B, Stone R, Deluisi J, Snider J (1995). A comparison of columnar water-vapor retrievals obtained with near-IR solar radiometer and microwave radiometer measurements. J Appl Meteorol, 34(6): 1384–1391

Reagan J, Pilewskie P, Herman B, Ben-David A (1987b). Extrapolation of Earth-based solar irradiance measurements to exoatmospheric levels for broad-band and selected absorption-band observations. IEEE Trans Geosci Rem Sens, GE-25(6): 647–653

Reagan J A, Thome K, Herman B, Gall R (1987a). Water vapor measurements in the 0.94 micron absorption band: Calibration, measurements, and data applications. In: Proceedings, International Geoscience and Remote Sensing Symposium, '87 Symposium, Ann Arbor, Mich. IEEE, 63–67

Schmid B, Hegg D A, Wang J, Bates D, Redemann J, Russell P B, Livingston J M, Jonsson H H, Welton E J, Seinfeld J H, Flagan R C, Covert D S, Dubovik O, Jefferson A (2003). Column closure studies of lower tropospheric aerosol and water vapor during ACE-Asia using airborne Sun photometer and airborne in situ and ship-based lidar measurements. J Geophys Res, 108(D23): 8656-8677

Schmid B, Michalsky J J, Slater D W, Barnard J C, Halthore R N, Liljegren J C, Holben B N, Eck T F, Livingston J M, Russell P B, Ingold T, Slutsker I (2001). Comparison of columnar water-vapor measurements from solar transmittance methods. Appl Opt, 40(12): 1886–1896

Schmid B, Spyak P R, Biggar S F, Wehrli C, Sekler J, Ingold T, Matzler C, Kampfer N (1998). Evaluation of the applicability of solar and lamp radiometric calibrations of a precision Sun photometer operating between 300 and 1025 nm. Appl Opt, 37(18): 3923–3941

Schmid B, Thome K J, Demoulin P, Peter R, Matzler C, Sekler J (1996). Comparison of modeled and empirical approaches for retrieving columnar water vapor from solar transmittance measurements in the 0.94 mm region. J Geophys Res, 101(9): 345–349, 358

Schmid B, Wehrli C (1995). Comparison of Sun photometer calibration by use of the Langley technique and the standard lamp. Appl Opt, 34 (21): 4500–4512, 512

Seckmeyer G, Bernhard G (1993). Cosine error correction of spectral UV irradiances. In: Stamnes K H, ed. Atmospheric Radiation, Proc. SPIE, 2049: 140–151

Shaw G E (1976). Error analysis of multi-wavelength sun photometry. Pure Appl Geophys, 114(1): 1–14

Shaw G E (1982). Solar spectral irradiance and atmospheric transmission at Mauna Loa Observatory. Appl Opt, 21(11): 2007–2011

Shiobara M, Spinhirne J D, Uchiyama A, Asano S (1996). Optical depth measurements of aerosol, cloud, and water vapor using Sun photometers during FIRE Cirrus IFO II. J Appl Meteorol, 35(1): 36–46

Slusser J, Gibson J, Bigelow D, Kolinski D, Disterhoft P, Lantz K, Beaubien A (2000). Langley method of calibrating UV filter radiometers. J Geophys Res, 105(D4): 4841–4849

Smirnov A, Holben B N, Eck T F, Dubovik O, Slutsker I (2000). Cloud screening and quality control algorithms for the AERONET database. Remote Sens Environ, 73(3): 337–349

Teramura A H, Sullivan J H, Ziska L H (1990). Interaction of elevated ultraviolet-B radiation and CO_2 on productivity and photosynthetic

characteristics in wheat, rice, and soybean. Plant Physiol, 94(2): 470–475

Thomason L W, Herman B M, Reagan J A (1983). The effect of atmospheric attenuators with structured vertical distributions on air mass determinations and Langley plot analysis. J Atmos Sci, 40(7): 1851–1854

Thome K J, Herman B, Reagan J (1992). Determination of precipitable water from solar transmission. J Appl Meteorol, 31(2): 157–165

Thome K J, Smith M W, Palmer J M, Reagan J A (1994). Three-channel solar radiometer for the determination of atmospheric columnar water vapor. Appl Opt, 33(24): 5811–5819

Thuillier G, Hers M, Simon P C, Labs D, Mandel H, Gillotay D (1998). Observation of the solar spectral irradiance from 200 to 870 nm during the ATLAS 1 and ATLAS 2 mission by the SOLSPEC spectrometer. Metrologia, 35(4): 689–695

Vanden Berghen F, Bersini H (2005). CONDOR, a new parallel, constrained extension of Powell's UOBYQA algorithm: experimental results and comparison with the DFO algorithm. Journal of Computational and Applied Mathematics, 181(1): 157–175

Wielicki B A, Cess R D, King M D, Randall D A, Harrison E F (1995). Mission to Planet Earth: role of clouds and radiation in climate. Bull Am Meteorol Soc, 76: 2125–2153

Willson R C, Mordvinov A V (2003). Secular total solar irradiance trend during solar cycles 21–23. Geophys Res Lett, 30(5): 1199–1202

Wilson S R, Forgan B W (1995). In situ calibration technique for UV spectral radiometers. Appl Opt, 34: 5475–5484

Yin B, Min Q, Duan M, Bartholomew M J, Vogelmann A M, Turner D D (2011). Retrievals of cloud optical depth and effective radius from Thin-Cloud Rotating Shadowband Radiometer measurements. J Geophys Res, 116(D23): D23208